

Organic compounds from macroalgal emission dominate new particle growth initiated by iodine species in coastal atmosphere

Yibei Wan^{1,1}, Xiangpeng Huang^{2,2}, Chong Xing^{1,1}, Qiongqiong Wang^{3,3}, Xinlei Ge^{2,2}, and Huan Yu^{1,1}

¹China University of Geosciences

²Nanjing University of Information Science & Technology

³The Hong Kong University of Science and Technology

December 1, 2022

Abstract

Iodine-initiated new particle formation (I-NPF) has long been recognized in coastal hotspot regions. However, no prior work has studied the exact chemical composition of organic compounds and their role in the coastal I-NPF. Here we present an important complementary study to the ongoing laboratory and field researches of iodine nucleation in coastal atmosphere. Oxidation and NPF experiments with vapor emissions from real-world coastal macroalgae were simulated in a bag reactor. On the basis of comprehensive mass spectrometry measurements, we reported for the first time a series of volatile precursors and their oxidation products in gas and particle phases in such a highly complex system. Organic compounds overwhelmingly dominated over iodine in the new particle growth initiated by iodine species. The identity and transformation mechanisms of organic compounds were identified in this study to provide a more complete story of coastal NPF from low-tide macroalgal emission.

Supporting Material for “**Chemical characterization of organic compounds involved in iodine-initiated new particle formation from coastal macro-algal emission**”

Yibei Wan¹, Xiangpeng Huang², Chong Xing¹, Qiongqiong Wang¹, Xinlei Ge², Huan Yu^{1,*}

¹ School of Environmental Studies, China University of Geosciences, Wuhan, 430074, China

² Jiangsu Key Laboratory of Atmospheric Environment Monitoring and Pollution Control, Collaborative Innovation Center of Atmospheric Environment and Equipment Technology, School of Environmental Science and Engineering, Nanjing University of Information Science and Technology, Nanjing 210044, China

* To whom correspondence should be addressed: yuhuan@cug.edu.cn

Text S1. The measurement details of GC-MS and FIGAERO-iodide-CIMS

GC-MS

300 milliliters of air sample from the canister was pulled through a cryogenic trap in the quadrupole GC-MS system (model TH-300B) and cooled to -160 °C for pre-concentration. After being trapped, the concentrated VOCs were flash desorbed by heating to 100 °C and transferred to a DB-624 column (60 m×0.25 mm×1.4 μm). CO₂ and moisture are removed before injection. The initial temperature for the chromatographic column was 41 °C, maintained for 6 min, and then raised to 180 °C at a rate of 6 °C min⁻¹. Qualitative identification of VOCs was performed using a full MS scan from 50 to 500 Th. The most probable identity of an analyte was obtained based on the first ranked matching by comparing with the reference mass spectra in the NIST library.

FIGAERO-iodide-CIMS

A sample flow was directly drawn into a turbulent flow ion-molecule reactor (IMR). Gaseous products were ionized as their corresponding adduct ions with I^- . Particulate products collected on the PTFE membrane filter were desorbed by a flow of heated UHP N_2 . The temperature of the N_2 increased from 20 to 200 °C in 50 min. The desorbed molecules entered the IMR and were charged by the same ionization mechanism. Background HNO_3 was inevitable in the experimental apparatus containing macroalgae and natural seawater. So the cluster ions containing NO_3^- or HNO_3 were observed occasionally. ToF-MS was configured to measure singly charged molecular ions of 7-720 Th with a MS resolution of ~ 4500 . Mass calibration was conducted using the ions of NO_3^- , CF_3O^- , $C_2F_3O_2^-$, $C_3F_5O_2^-$, I_3^- for gaseous products and NO_3^- , I^- , $IHNO_3^-$, $IC_2F_3HO_2^-$, I_3^- for particulate products. Reliable formula identification of ion peaks was corroborated by high accuracy of fits (<20 ppm) and isotope patterns. Background signal in the gas phase was determined by measuring a UHP N_2 flow. The signal during the last 3 minutes of the soak period of PTFE membrane filter was regarded as background signal in the particle phase. Background signals were then subtracted from the intensities of compound formulas.

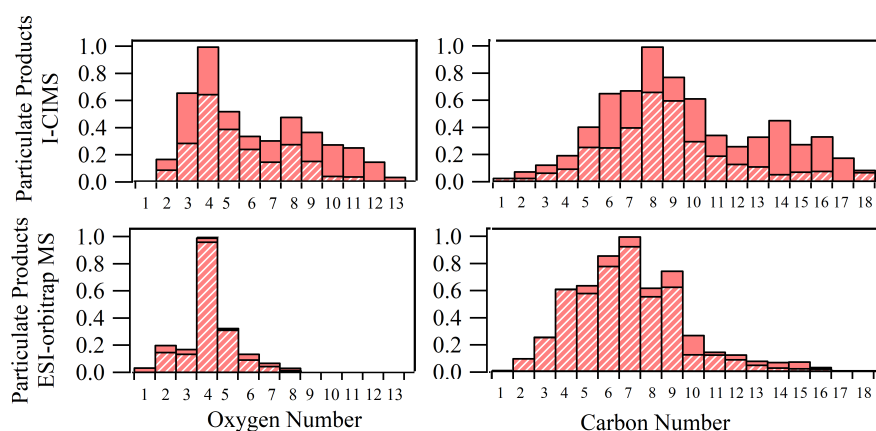


Figure S1. Oxygen and carbon atom number distributions of particulate products measured by iodide-CIMS and ESI-orbitrap MS in a typical ozonolysis experiment (dynamic mode). Hatched bars indicate the fractions of formulas observed by both mass spectrometers.

Hosted file

si_acp.docx available at <https://authorea.com/users/560450/articles/608457-organic-compounds-from-macroalgal-emission-dominate-new-particle-growth-initiated-by-iodine-species-in-coastal-atmosphere>

Chemical characterization of organic compounds involved in iodine-initiated new particle formation from coastal macro-algal emission

Yibei Wan¹, Xiangpeng Huang², Chong Xing¹, Qiongqiong Wang¹, Xinlei Ge², Huan Yu^{1,*}

¹ School of Environmental Studies, China University of Geosciences, Wuhan, 430074, China

² Jiangsu Key Laboratory of Atmospheric Environment Monitoring and Pollution Control, Collaborative Innovation Center of Atmospheric Environment and Equipment Technology, School of Environmental Science and Engineering, Nanjing University of Information Science and Technology, Nanjing 210044, China

* To whom correspondence should be addressed: yuhuan@cug.edu.cn

Abstract

Iodine-initiated new particle formation (I-NPF) has long been recognized in coastal hotspot regions. However, no prior work has studied the exact chemical composition of organic compounds and their role in the coastal I-NPF. Here we present an important complementary study to the ongoing laboratory and field researches of iodine nucleation in coastal atmosphere. Oxidation and NPF experiments with vapor emissions from real-world coastal macroalgae were simulated in a bag reactor. On the basis of comprehensive mass spectrometry measurements, we reported for the first time a variety of volatile precursors and their oxidation products in gas and particle phases in such a highly complex system. Organic compounds overwhelmingly dominated over iodine in the new particle growth initiated by iodine species. The identity and transformation mechanisms of organic compounds were identified in this study to provide a more complete story of coastal NPF from low-tide macroalgal emission.

1. Introduction

Coastal new particle formation (NPF) may be driven by daytime low-tide emission of iodine species from macroalgae fully or partially exposed to the air. The phenomenon was reported in hotspot locations of west Europe, Australia and polar regions (Allan et al., 2015; Baccarini et al., 2020; Beck et al., 2021; Heard et al., 2006; McFiggans et al., 2010; O'Dowd et al., 2002; Sipil et al., 2016; Whitehead et al., 2009). In the southeast coastline of China, we reported intense iodine-initiated NPF based on particle number size distribution and iodine measurements (Yu et al.,

2019).

To simulate iodine-initiated NPF (I-NPF) in controlled laboratory conditions, I_2 or CH_2I_2 vapor was usually photolyzed in the presence of ozone to provide nucleation precursors (Burkholder et al., 2004; He et al., 2021; Huang et al., 2022; Jimenez et al., 2003; Martín et al., 2020; Monahan et al., 2012; O'Dowd et al., 2004; Saunders and Plane, 2005). Ashu-Ayem et al. (2012); McFiggans et al. (2004); Monahan et al. (2012); Sellegri et al. (2005) and Sellegri et al. (2016) also investigated the NPF from the vapors emitted by real-world macroalgal specimens or seawater in laboratory chamber or apparatus. However, the focus of all above studies are emission rate, oxidation mechanisms or nucleation pathways of iodine species. For example, positive correlations between particle concentrations and I_2 or CH_2I_2 mixing ratios were usually observed (Burkholder et al., 2004; Jimenez et al., 2003; Monahan et al., 2012; Sellegri et al., 2005). Kinetic studies in flow tube or CERN CLOUD chamber proposed the clustering of iodine oxides (I_xO_y) or iodine oxoacids (HIO_3 , HIO_2) as nucleation mechanisms on the basis of photoionization TOF-MS (Martín et al., 2020), Api-TOF and nitrate-Chemical Ionization Mass Spectrometer (CIMS) measurements (He et al., 2021). A recent chamber study showed heterogeneous reaction between iodine oxide nanoparticle, meso-erythritol (or glyoxal) and dimethylamine accelerated nanoparticle growth (Huang et al., 2022).

Until now, no prior work has investigated the exact chemical identity of organic compounds (other than iodinated methane) and their role in I-NPF. The role of biogenic terpenes and anthropogenic aromatics in continental NPF has been recognized for a long time (Donahue et al., 2013). Their ozonolysis or photochemistry products have been investigated in depth by using Electrospray Ionization Mass Spectrometry (ESI-MS) and more recently, CIMS (Ehn et al., 2014; Faxon et al., 2018; Kundu et al., 2012; Kundu et al., 2017; Nguyen et al., 2010; Riva et al., 2017; Wang et al., 2020; Yan et al., 2020). It is very likely that certain volatile organic compounds (VOCs) emitted mutually with iodine or iodinated methane from coastal biota or biologically active sea surface may also be involved in coastal I-NPF process and promote the growth of iodine particles.

To test this hypothesis, we conducted oxidation and NPF experiments with vapor emissions from real-world coastal macroalgae in a bag reactor. A suite of mass spectrometric methods including Inductively Coupled Plasma-MS (ICP-MS), Gas Chromatography-MS (GC-MS), iodide-CIMS and ESI-orbitrap MS were applied to measure vapor precursors, gaseous products and particulate products during the NPF process. Mass concentrations of total organic carbon (TOC) and total iodine (TI) of new particles were compared to evaluate the relative importance of organics and iodine in new particle growth. The identity and transformation mechanisms of organic compounds were identified to provide a more complete story of coastal NPF from low-tide macroalgal emission. Our

study is thus complementary to prior laboratory and field studies of I-NPF, but has an emphasis on organics.

2. Experiments

2.1 Experimental apparatus and sample collection

Similar to Potential Aerosol Mass (PAM) Oxidation Flow Reactor, a bag reactor was designed to provide an oxidizing environment for simulating atmospheric oxidation processes of algae-emitted VOCs. The bag reactor was made from 75 μm -thick fluorinated ethylene propylene (FEP) Teflon (1.2 m \times 1.5 m, flat dimension). The volume of the bag at full inflation was determined experimentally to be about 200 L. The bag was suspended vertically (Figure 1) and kept in the dark or directly exposed to room light of fluorescent lamp. Because the purpose of this study is to qualitatively measure the oxidation products of algae-emitted VOCs, wall loss, production rate and other kinetic factors in the bag reactor were not evaluated. Fresh macroalgae (*Undaria pinnatifida*) was collected from intertidal zone at Xiangshan gulf of east China coast and stored at -10 $^{\circ}\text{C}$ until the experiments. 2 kg macroalgae was put in a 20 L Pyrex glass bottle that was filled with \sim 1 L natural seawater. The specimens was partially exposed to the air to simulate tidal emersion of macroalgae. A flow of particle-free ultra high purity (UHP) air blew algae-emitted VOCs out of the bottle and merged with a diluting air flow before entering the bag reactor.

Two types of experiments were conducted. In the three ozonolysis experiments, ozone (O_3) was generated by flowing an UHP air flow through a 5 Watts 185 nm UV lamp. The O_3 flow was fed just before the bag reactor was fully inflated. Final O_3 concentration in the bag reactor was measured to be \sim 200 ppbv using an ozone analyzer (Model 49i, Thermo-Fisher Scientific Inc.). In an additional OH-enhanced experiment, the O_3 /VOC mixture flow was directed through a 254 nm UV light before entering the bag reactor. OH radicals were produced via the reaction $\text{O}_3+h\nu\rightarrow\text{O}_2+\text{O}(^1\text{D})$ and $\text{O}(^1\text{D})+\text{H}_2\text{O}\rightarrow 2\text{OH}$.

Before each experiment, the bag was purged for several hours to reduce background particle concentrations to below 1 cm^{-3} . The bag reactor was first operated in a static mode to monitor the time evolution of gaseous products and particle size, and then in a dynamic mode to collect enough particles for offline chemical analysis. In the static mode, the bag was first filled to full inflation with the VOCs/ O_3 flows. The flows were then shut down; a Scanning Mobility Particle Sizer (SMPS, model 3936, TSI Inc., Shoreview, MN, USA) and an Aerodyne iodide-CIMS pulled two flows of 0.3 liters per minute (lpm) and 1.8 lpm out of the bag, respectively. The SMPS measured the particle

number size distribution from 14 to 600 nm.

In the dynamic mode, the VOCs/O₃ flow of 3 lpm was fed to the bag continuously, while the SMPS and a vacuum pump (GAST Group Ltd.) pulled sample flows of 0.3 and 2.7 lpm, respectively, out of the bag reactor. This resulted in an overall residential time of 67 minutes for the O₃/VOC mixture in the fully inflated bag. The particles in the 2.7 lpm sample flow were collected onto a Zefluor® PTFE membrane filter mounted in a filter inlet for gases and aerosols (FIGAERO) for iodide-CIMS analysis, or alternatively, onto 47 mm diameter double quartz fiber filter pack mounted in a filter holder for ESI-orbitrap MS, ICP-MS and TOC analysis. The front filter of the double filter pack collected the particles, while the back filter placed downstream of the front filter was supposed to adsorb the same amount of volatile species as the front filter.

2.2 Chemical analysis

Before the ozonolysis experiments, the algae-emitted VOCs in the bag reactor was collected by a 6-liter pre-evacuated stainless-steel canisters (Entech Instruments, Inc., Simi Valley, CA, USA) and was analyzed using a quadrupole GC-MS system (model TH-300B, Wuhan Tianhong Instruments Co. Ltd., Wuhan, China). The algae-emitted VOCs, as well as their gaseous and particulate products, were also measured by the FIGAERO-iodide-CIMS. Iodide-adduct chemical ionization is well suited for measuring oxygenated or acidic compounds with minimal fragmentation. More details of the GC-MS and FIGAERO-iodide-CIMS measurements can be found in Supporting Material. The theory and design of the two instruments were described by Wang et al. (2014) and Lopez-Hilfiker et al. (2014).

The particles collected on quartz fiber filters were sent for offline quantification of TOC and TI, as well as non-target analysis of organic compounds using ESI-orbitrap MS. The front and back filters were treated, separately, following the procedure as below: the filter was ultrasonicated twice with 10-mL water and acetone nitrile solvent mixture (v:v=1:1). The extract was filtered by a 0.2 µm PTFE syringe filter and evaporated in a rotary evaporator to 0.5 mL. After being centrifuged for 30 min at 12000 rpm, the supernatant was collected for TI analysis by Agilent 1100 HPLC-7900 ICP-MS (Agilent Technologies, Santa Clara, CA, USA) and TOC analysis by a TOC analyzer (Model TOC-5000A, Shimadzu, Japan). TI or TOC in the particles was obtained by subtracting the amount on the back filter from that on the front filter. Nontarget analysis of organic compounds in the supernatant was conducted using a Q Exactive hybrid Quadrupole-Orbitrap mass spectrometer (Thermo Scientific, Bremen, Germany). The supernatant was directly infused by a syringe pump and ionized in negative ESI source. All the ions in the m/z range from 50 to 500 Th were scanned with a

mass resolution of 70000. The chemically sound CHO molecular formulas were computed with a mass tolerance of ± 2 ppm for these ions. Only the compounds that existed solely in the front filter or with ion intensity in the front filter higher than that in the back filter by a factor of 3 were regarded as the organic compounds in the particle phase.

3. Results and discussion

3.1 Relative mass contribution of organic carbon and iodine to new particles

Typical banana-shape particle size spectrum observed in the static mode of an ozonolysis experiment is shown in Figure 2a. In the presence of room light, new particles larger than 14 nm were observed only 58 minutes after the injection of ozone flow. This relative long time is due to the build-up of O₃ concentration and subsequent accumulation of oxidation products. No particles were formed in the absence of room light or ozone. In the dynamic mode experiments, O₃ in the bag reactor was kept at its maximum concentration 200 ppbv. With a prolonged residential time of 67 min, the particles grew to 102 ± 23 nm, which was measured by the SMPS at the outlet of the bag reactor. The TOC and TI measurements show that organic compounds contributed more particle mass than iodine with TOC/(I+TOC) ratio of $96.1 \pm 2.9\%$ (Table 1).

In the OH-enhanced experiment (dynamic mode), more particulate products were generated with enhanced oxidation capacity: TI in the particles increased by a factor of 10.8; TOC increased by a factor of 2.7; particle number concentration increased by a factor of 7.4. On the other hand, particle size decreased to 73 nm and TOC/(TI+TOC) ratio decreased to 92.9% (Table 1). These differences indicate that more iodine nuclei were produced with enhanced OH concentration, probably via $\text{OIO} + \text{OH} \rightarrow \text{HOIO}_2$ (Plane et al., 2006). Competitive uptake of condensing organic vapors onto these iodine nuclei limited the growth of individual new particles. Nevertheless, organic compounds overwhelmingly dominated over iodine in the mass contribution to new particle growth.

The significant organic contribution observed in the laboratory condition is generally consistent with TOC/(I+TOC) ratio of 98.2% in 10-56 nm new particles collected during a coastal I-NPF event in China (Yu et al., 2019), although TOC and TI during the field event are two orders of magnitude lower than those in the bag reactor (Table 1). Mean diameter of new particles was observed to be only 16 nm during the field event. But those small new particles are expected to grow into CCN active sizes, given longer residence time and uptake of more condensing vapors in the atmosphere.

3.2 Macroalgal emission

It is of particular interest to know what VOCs are emitted from coastal macroalgae. They are potential precursors of iodine particle nucleation and growth. The canister sampling followed by GC-MS analysis showed that the top 9 non-CHO compounds with highest TIC peak areas (Table 2) are C₅ alkanes, C₁₀ alpha-pinene and halogenated C₁, C₃ and C₅ alkanes. The top 10 CHO compounds are C₂-C₆ alcohols and carbonyls with saturated or unsaturated carbon chain.

Iodide-CIMS is more sensitive to more oxygenated or acidic compounds and thus complementary to the GC-MS measurement. The 76 organic precursors detected by iodide-CIMS before ozone addition were characterized by C_{1,2,3,6} and O₂₋₃ formulas (Figure 3a). The top 7 compounds with highest ion intensities were CH₂O₂, C₂H₄O₂, C₃H₆O₃, C₆H₁₀O₃, C₂H₆O₂, C₄H₈O₂ and C₆H₁₂O₃, which accounted for 82.5% of total ion intensity. They are C₁-C₆ mono-carboxylic acids, hydroxyl carboxylic acids or oxo-carboxylic acids with 2 to 3 oxygen atoms (Table 2). Their carbon atom numbers are in general consistent with the VOCs detected by GC-MS.

Relatively high signals of HNO₃ were observed as NO₃⁻ and HNO₃I⁻ before the addition of ozone to the bag reactor. Because HNO₃ and HNO₂ were also observed as deprotonated ions or I⁻ clusters in the particle phase during the NPF, HNO₃ is also an important precursor of particle formation.

3.3 Gaseous and particulate products

3.3.1 Inorganic molecules and radicals

Being different from nitrate-CIMS, our iodide-CIMS did not detect nucleating clusters of iodine oxides or oxyacids after the addition of ozone. Instead, dozens of new inorganic molecules or radicals were observed as clusters with I⁻, NO₃⁻ or deprotonated ions in the gas or particle phase (Figure 4). We grouped these species by elemental composition and investigated their role in the NPF by observing how their gaseous ion intensities evolved during the NPF event in the bag reactor (Figure 2b-2f).

1. Cl, I, Cl₂ and ClI in the gas phase: the intensities of I and Cl increased ca. 10 minutes before 14 nm particles appeared and decreased as the particles grew up. Based on prior work of Burkholder et al. (2004); Jimenez et al. (2003); O'Dowd et al. (2004), we suggested the photolysis of CH₂Cl₂, CHBrCl, CH₃I and C₃H₇I was the source of halogen atoms (e.g., CH₃I+hν→CH₃+I). There was a time lag of 20-25 minutes between the appearances of Cl and I and those of ClI and Cl₂, which were probably from the recombination of Cl and I atoms.

2. IO₂, IO, ClIO, INO₂ and ClNO₂ in the gas phase: these species showed a similar time series to I and Cl atoms. IO, IO₂ and ClIO could be from the reactions between I, ClI and O₃. INO₂ is usually thought to form upon the reaction I+NO₂+M →INO₂+M (Saiz-Lopez et al., 2012). ClNO₂ was likely to form upon similar reaction between Cl and NO₂ in the bag reactor.

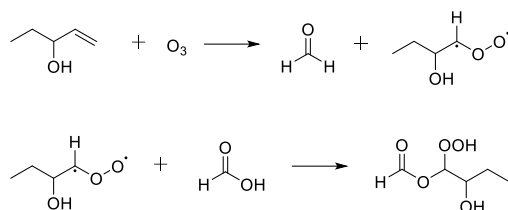
3. HIO₃ and INO₃: the two species seem to be the end products of above intermediates, because their intensities kept on increasing during new particle growth. INO₃, which is iodine nitrate IONO₂, was detected in both gas and particle phases. IONO₂ probably formed upon the recombination of IO and NO₂ (IO+NO₂+M→IONO₂+M) (Saiz-Lopez et al., 2012). HIO₃ was likely to form via OIO+OH→HOIO₂ or I + H₂O + O₃→HOIO₂ + OH (Martín et al., 2020; Plane et al., 2006). HIO₃ was not detected in particle phase by iodide-CIMS, which is contrary to the observation by HPLC-ICP-MS that total iodine was mostly dominated IO₃⁻ peak. The signals of IO⁻, IO₂⁻ and HIONO₃⁻ in the particle phase are therefore most likely to result from thermal decomposition of HIO₃ to HIO and HIO₂ in the FIGAERO thermal desorption process.

4. CH₃SO₃H, S₂⁻, S₃⁻, SO₃⁻: We observed methane sulfonic acid (CH₃SO₃H, MSA) in both gas and particle phases. Gaseous MSA increased in the beginning, but decreased after new particles appeared (Figure 2f). Apparently, our measurement suggested MSA contributed to the growth of new particles, but it is unknown if it also participated in nucleation. We suggested S₂⁻, S₃⁻, SO₃⁻ ions observed in the particle phase were thermal decomposition products of MSA.

3.3.2 Gaseous organic products

After ozone addition, a gradual transformation from C₁-C₃ precursors to C₅-C₈ gaseous products was observed during the NPF process (Figure 2h). In the meanwhile, the oxygen atom number of the compounds increased from 2-3 to 4-7 (Figure 2g). The formation of compounds with more carbon atoms than the parent VOCs is unlikely in the gas phase, except bimolecular reactions of stabilized Criegee intermediates (SCIs) that typically form upon alkene ozonolysis. Similar to isoprene ozonolysis (Inomata et al., 2014; Riva et al., 2017), we propose the SCI addition mechanism can also explain the transformation observed in our case: (1) C₄ SCIs formed upon the ozonolysis of CHO precursors with C=C double bonds (e.g., those observed by GC-MS in Table 2). (2) the insertion of C₄ SCIs into carboxylic acid precursors (e.g., those observed by CIMS in Table 2) produced oligomeric hydroperoxides. An example was shown in Scheme I for the reactions of most abundant ethyl vinyl carbinol (C₅H₁₀O), ozone and formic acid (CH₂O₂), but the same mechanism is also applicable for ethyl vinyl ketone (C₅H₈O) and other abundant C₂-C₅ carboxylic acids and hydroxyl carboxylic acids. As a result, a series of gaseous oligomeric hydroperoxides C₅H₁₀O₅,

219 C₆H₁₀O₅, C₆H₁₂O₅, C₇H₁₂O₆, C₇H₁₄O₆, C₈H₁₄O₅, C₈H₁₆O₆, C₈H₁₆O₅ and C₉H₁₆O₆ were observed with
 220 high intensity by iodide-CIMS.



Scheme I

221 3.3.3 Particulate organic products

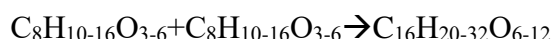
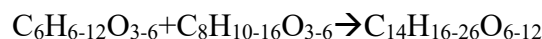
223 In the end of a typical ozonolysis experiment (dynamic mode), 100 and 364 new formulas were
 224 observed in the gas and particle phases, respectively, including 73 semi-VOCs appeared in both gas
 225 and particle phases. Those semi-VOCs accounted for 81 and 20% of total ion intensities of gaseous
 226 and particulate products, respectively. Being different from unimodal atom number distributions of
 227 gaseous products ($C_{\text{max}} = 7$ and $O_{\text{max}} = 5$, Figure 3b), particulate products were characterized by
 228 distinct bimodal or trimodal distribution of carbon number ($C_{\text{max}} = 8, 14$ and 16 , Figure 3c) and
 229 oxygen number ($O_{\text{max}} = 4$ and 8), implying possible dimer formation via accretion reactions in the
 230 particle phase.

231 ESI-Orbitrap MS differs from FIGAERO-iodide-CIMS in extraction method (ultrasonic solvent
 232 extraction from quartz fiber filter *vs.* thermal desorption from PTFE membrane filter), ionization
 233 source (electrospray ionization *vs.* iodide-adduct chemical ionization) and MS resolving power
 234 (70000 *vs.* 4500). The result showed that ESI-orbitrap MS and FIGAERO-iodide-CIMS detected 336
 235 and 364 organic formulas, respectively, in the particle phase. 167 organic formulas were commonly
 236 observed by both methods, which accounted for 87% and 54% of total ion intensity of organic
 237 formulas by the two methods, respectively (Figure S1). As shown in Figure 3c and 3d,
 238 FIGAERO-iodide-CIMS had better sensitivity toward the organic compounds with more oxygen
 239 atoms (e.g., $O \geq 8$) and carbon atoms (e.g., $C \geq 10$). As a result, bimodal carbon and oxygen atom
 240 number distributions were observed by FIGAERO-iodide-CIMS, but not ESI-orbitrap MS.

241 The measurement by ESI-orbitrap MS provided more insights about the formation mechanism of
 242 particulate products. We compared the 336 formulas detected by ESI-orbitrap MS in our study with
 243 the 414 formulas of isoprene ozonolysis SOA products (Nguyen et al., 2010) and 922 formulas of
 244 alpha-pinene ozonolysis SOA products (Putman et al., 2012) measured by the ESI-orbitrap MS. It
 245 was found that 72% of the formulas in this study can also be found in isoprene SOA, but only 39%
 246 can be found in alpha-pinene SOA. This seems to imply that some similar alkene ozonolysis

reactions occurred in our system and isoprene ozonolysis.

For such a highly complex system full of various algae-emitted precursors, it is impossible to simply propose a reaction mechanism to explain the formation of all particulate products, nor to list all reactions occurring in the bag reactor. On the basis of particle-phase oligomer chemistry (Seinfeld and Pandis, 2016), especially the well-understood isoprene ozonolysis SOA chemistry (Inomata et al., 2014; Nguyen et al., 2010; Riva et al., 2017), we suggest a variety of accretion reactions without uniform oligomerization pattern (e.g., esterification, aldol condensation, hemiacetal reactions, peroxyhemiacetal formation and SCI reactions, etc.) transformed $O_{\max}=4$ and $C_{\max}=8$ multifunctional monomers (like alcohols, carbonyls, hydroperoxides, carboxylic acids) to $O_{\max}=8$ and $C_{\max}=14$ or 16 dimers. Scheme II illustrated addition type self- and cross-oligomerization between C_6 and C_8 monomers produces C_{14} and C_{16} dimers. All the formulas in Scheme II are among the most abundant ones observed in the particle phase by the iodide-CIMS.



Scheme II

4. Conclusions

Using a suite of mass spectrometers, we reported, for the first time, the chemical compositions of volatile precursors emitted by real-world coastal macroalgae and their gaseous and particulate oxidation products. In the presence of room light and ozone, the photolysis of halogenated $C_{1,3,5}$ alkanes ends up as HIO_3 and INO_3 . It was most likely HIO_3 initiated NPF and provided nuclei for the further condensation of other products like INO_3 , MSA and CHO compounds. Gas-phase SCI reactions and particle-phase accretion reactions transformed C_1 - C_6 and O_2 - O_3 precursors gradually to particulate products with $C_{\max}=8, 14$ and 16 and $O_{\max}=4$ and 8. As a result, organic carbon were found to overwhelmingly dominated over iodine in the mass contribution to the new particle growth. Although our instruments did not allow the detection of nucleating clusters of iodine oxides or oxyacids, our study provided important complementary information to the ongoing laboratory and field researches of coastal I-NPF.

Data Availability Statement

All data related to figures and tables in this study are archived and made available through Zenodo data repository <https://doi.org/10.5281/zenodo.6965859>.

276 **Acknowledgement**

277 This work was supported by the National Science Foundation of China (grant no. 41975831 and
278 42175131) and Start-up research funding from China University of Geosciences.

279 **References**

- 280 Allan, J. D., et al. (2015), Iodine observed in new particle formation events in the Arctic atmosphere
281 during ACCACIA, *Atmos. Chem. Phys.*, *15*(10), 5599-5609, doi:10.5194/acp-15-5599-2015.
- 282 Ashu-Ayem, E. R., U. Nitschke, C. Monahan, J. Chen, S. B. Darby, P. D. Smith, C. D. O'Dowd, D. B.
283 Stengel, and D. S. Venables (2012), Coastal Iodine Emissions. 1. Release of I₂ by *Laminaria*
284 *digitata* in Chamber Experiments, *Environmental Science & Technology*, *46*(19), 10413-10421,
285 doi:10.1021/es204534v.
- 286 Baccarini, A., et al. (2020), Frequent new particle formation over the high Arctic pack ice by
287 enhanced iodine emissions, *Nature Communications*, *11*(1), 4924,
288 doi:10.1038/s41467-020-18551-0.
- 289 Beck, L. J., et al. (2021), Differing Mechanisms of New Particle Formation at Two Arctic Sites,
290 *Geophysical Research Letters*, *48*(4), e2020GL091334, doi:<https://doi.org/10.1029/2020GL091334>.
- 291 Burkholder, J. B., J. Curtius, A. R. Ravishankara, and E. R. Lovejoy (2004), Laboratory studies of
292 the homogeneous nucleation of iodine oxides, *Atmospheric Chemistry and Physics*, *4*(1), 19-34,
293 doi:10.5194/acp-4-19-2004.
- 294 Donahue, N. M., et al. (2013), How do organic vapors contribute to new-particle formation?,
295 *Faraday Discussions*, *165*(0), 91-104, doi:10.1039/C3FD00046J.
- 296 Ehn, M., et al. (2014), A large source of low-volatility secondary organic aerosol, *Nature*, *506*(7489),
297 476-479, doi:10.1038/nature13032.
- 298 Faxon, C., J. Hammes, M. Le Breton, R. K. Pathak, and M. Hallquist (2018), Characterization of
299 organic nitrate constituents of secondary organic aerosol (SOA) from nitrate-radical-initiated
300 oxidation of limonene using high-resolution chemical ionization mass spectrometry, *Atmospheric*
301 *Chemistry and Physics*, *18*(8), 5467-5481, doi:10.5194/acp-18-5467-2018.
- 302 He, X. C., et al. (2021), Role of iodine oxoacids in atmospheric aerosol nucleation, *Science*,
303 *371*(6529), 589-595, doi:10.1126/science.abe0298.
- 304 Heard, D. E., et al. (2006), The North Atlantic Marine Boundary Layer Experiment(NAMBLEX).
305 Overview of the campaign held at Mace Head, Ireland, in summer 2002, *Atmos. Chem. Phys.*, *6*(8),
306 2241-2272, doi:10.5194/acp-6-2241-2006.
- 307 Huang, R.-J., et al. (2022), Heterogeneous iodine-organic chemistry fast-tracks marine new particle
308 formation, *Proceedings of the National Academy of Sciences*, *119*(32), e2201729119,
309 doi:10.1073/pnas.2201729119.
- 310 Inomata, S., K. Sato, J. Hirokawa, Y. Sakamoto, H. Tanimoto, M. Okumura, S. Tohno, and T.
311 Imamura (2014), Analysis of secondary organic aerosols from ozonolysis of isoprene by proton
312 transfer reaction mass spectrometry, *Atmospheric Environment*, *97*, 397-405,
313 doi:<https://doi.org/10.1016/j.atmosenv.2014.03.045>.
- 314 Jimenez, J. L., R. Bahreini, D. R. Cocker III, H. Zhuang, V. Varutbangkul, R. C. Flagan, J. H.
315 Seinfeld, C. D. O'Dowd, and T. Hoffmann (2003), New particle formation from photooxidation of
316 diiodomethane (CH₂I₂), *Journal of Geophysical Research: Atmospheres*, *108*(D10),
317 doi:<https://doi.org/10.1029/2002JD002452>.
- 318 Kundu, S., R. Fisseha, A. L. Putman, T. A. Rahn, and L. R. Mazzoleni (2012), High molecular
319 weight SOA formation during limonene ozonolysis: insights from ultrahigh-resolution FT-ICR
320 mass spectrometry characterization, *Atmos. Chem. Phys.*, *12*(12), 5523-5536,
321 doi:10.5194/acp-12-5523-2012.

322 Kundu, S., R. Fisseha, A. L. Putman, T. A. Rahn, and L. R. Mazzoleni (2017), Molecular formula
 323 composition of β -caryophyllene ozonolysis SOA formed in humid and dry conditions, *Atmospheric*
 324 *Environment*, 154, 70-81, doi:<https://doi.org/10.1016/j.atmosenv.2016.12.031>.
 325 Lopez-Hilfiker, F. D., et al. (2014), A novel method for online analysis of gas and particle
 326 composition: description and evaluation of a Filter Inlet for Gases and AEROsols (FIGAERO),
 327 *Atmospheric Measurement Techniques*, 7(4), 983-1001, doi:10.5194/amt-7-983-2014.
 328 Martín, J. C. G., T. R. Lewis, M. A. Blitz, J. M. C. Plane, M. Kumar, J. S. Francisco, and A.
 329 Saiz-Lopez (2020), A gas-to-particle conversion mechanism helps to explain atmospheric particle
 330 formation through clustering of iodine oxides, *Nature Communications*, 11(1), 4521,
 331 doi:10.1038/s41467-020-18252-8.
 332 McFiggans, G., et al. (2010), Iodine-mediated coastal particle formation: an overview of the Reactive
 333 Halogens in the Marine Boundary Layer (RHaMBLe) Roscoff coastal study, *Atmospheric*
 334 *Chemistry and Physics*, 10(6), 2975-2999, doi:10.5194/acp-10-2975-2010.
 335 McFiggans, G., et al. (2004), Direct evidence for coastal iodine particles from Laminaria macroalgae
 336 – linkage to emissions of molecular iodine, *Atmos. Chem. Phys.*, 4(3), 701-713,
 337 doi:10.5194/acp-4-701-2004.
 338 Monahan, C., E. R. Ashu-Ayem, U. Nitschke, S. B. Darby, P. D. Smith, D. B. Stengel, D. S. Venables,
 339 and C. D. O'Dowd (2012), Coastal Iodine Emissions: Part 2. Chamber Experiments of Particle
 340 Formation from Laminaria digitata-Derived and Laboratory-Generated I₂, *Environmental Science*
 341 *& Technology*, 46(19), 10422-10428, doi:10.1021/es3011805.
 342 Nguyen, T. B., A. P. Bateman, D. L. Bones, S. A. Nizkorodov, J. Laskin, and A. Laskin (2010),
 343 High-resolution mass spectrometry analysis of secondary organic aerosol generated by ozonolysis
 344 of isoprene, *Atmospheric Environment*, 44(8), 1032-1042,
 345 doi:<https://doi.org/10.1016/j.atmosenv.2009.12.019>.
 346 O'Dowd, C. D., J. L. Jimenez, R. Bahreini, R. C. Flagan, J. H. Seinfeld, K. Hämeri, L. Pirjola, M.
 347 Kulmala, S. G. Jennings, and T. Hoffmann (2002), Marine aerosol formation from biogenic iodine
 348 emissions, *Nature*, 417, 632, doi:10.1038/nature00775.
 349 O'Dowd, C. D., M. C. Facchini, F. Cavalli, D. Cebrunis, M. Mircea, S. Decesari, S. Fuzzi, Y. J. Yoon,
 350 and J.-P. Putard (2004), Biogenically driven organic contribution to marine aerosol, *Nature*, 431,
 351 676-680.
 352 Plane, J. M. C., D. M. Joseph, B. J. Allan, S. H. Ashworth, and J. S. Francisco (2006), An
 353 Experimental and Theoretical Study of the Reactions OIO + NO and OIO + OH, *The Journal of*
 354 *Physical Chemistry A*, 110(1), 93-100, doi:10.1021/jp055364y.
 355 Putman, A. L., J. H. Offenberg, R. Fisseha, S. Kundu, T. A. Rahn, and L. R. Mazzoleni (2012),
 356 Ultrahigh-resolution FT-ICR mass spectrometry characterization of α -pinene ozonolysis SOA,
 357 *Atmospheric Environment*, 46, 164-172, doi:<https://doi.org/10.1016/j.atmosenv.2011.10.003>.
 358 Riva, M., S. H. Budisulistiorini, Z. F. Zhang, A. Gold, J. A. Thornton, B. J. Turpin, and J. D. Surratt
 359 (2017), Multiphase reactivity of gaseous hydroperoxide oligomers produced from isoprene
 360 ozonolysis in the presence of acidified aerosols, *Atmospheric Environment*, 152, 314-322,
 361 doi:10.1016/j.atmosenv.2016.12.040.
 362 Saiz-Lopez, A., J. M. C. Plane, A. R. Baker, L. J. Carpenter, R. von Glasow, J. C. Gómez Martín, G.
 363 McFiggans, and R. W. Saunders (2012), Atmospheric Chemistry of Iodine, *Chemical Reviews*,
 364 112(3), 1773-1804, doi:10.1021/cr200029u.
 365 Saunders, R. W., and J. M. C. Plane (2005), Formation Pathways and Composition of Iodine Oxide
 366 Ultra-Fine Particles, *Environmental Chemistry*, 2(4), 299-303,
 367 doi:<https://doi.org/10.1071/EN05079>.
 368 Seinfeld, J. H., and S. N. Pandis (2016), *Atmospheric chemistry and physics: from air pollution to*
 369 *climate change*, 3rd ed., John Wiley and Sons. Inc., New York.
 370 Sellegri, K., et al. (2016), Evidence of atmospheric nanoparticle formation from emissions of marine
 371 microorganisms, *Geophysical Research Letters*, 43(12), 6596-6603,

doi:<https://doi.org/10.1002/2016GL069389>.

Sellegri, K., Y. J. Yoon, S. G. Jennings, C. D. O'Dowd, L. Pirjola, S. Cautenet, H. Chen, and T. Hoffmann (2005), Quantification of Coastal New Ultra-Fine Particles Formation from In situ and Chamber Measurements during the BIOFLUX Campaign, *Environmental Chemistry*, 2(4), 260-270, doi:<https://doi.org/10.1071/EN05074>.

Sipilä, M., et al. (2016), Molecular-scale evidence of aerosol particle formation via sequential addition of HIO₃, *Nature*, advance online publication, doi:10.1038/nature19314
<http://www.nature.com/nature/journal/vaop/ncurrent/abs/nature19314.html#supplementary-information>.

Wang, M., et al. (2020), Photo-oxidation of Aromatic Hydrocarbons Produces Low-Volatility Organic Compounds, *Environmental science & technology*, 54(13), 7911-7921, doi:10.1021/acs.est.0c02100.

Wang, M., et al. (2014), Development and validation of a cryogen-free automatic gas chromatograph system (GC-MS/FID) for online measurements of volatile organic compounds, *Analytical Methods*, 6(23), 9424-9434, doi:10.1039/C4AY01855A.

Whitehead, J. D., G. B. McFiggans, M. W. Gallagher, and M. J. Flynn (2009), Direct linkage between tidally driven coastal ozone deposition fluxes, particle emission fluxes, and subsequent CCN formation, *Geophysical Research Letters*, 36(4), doi:doi:10.1029/2008GL035969.

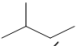

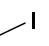
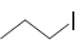
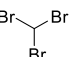
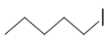
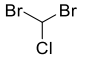
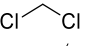
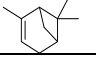
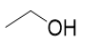
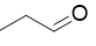
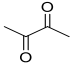
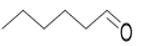
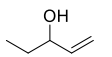
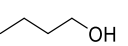
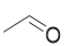
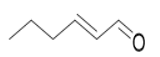
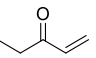
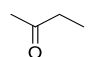
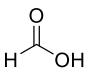
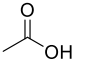
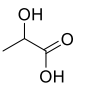
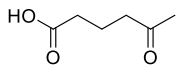
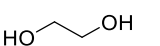
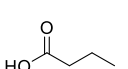
Yan, C., et al. (2020), Size-dependent influence of NO(x) on the growth rates of organic aerosol particles, *Science advances*, 6(22), eaay4945, doi:10.1126/sciadv.aay4945.

Yu, H., L. Ren, X. Huang, M. Xie, J. He, and H. Xiao (2019), Iodine speciation and size distribution in ambient aerosols at a coastal new particle formation hotspot in China, *Atmospheric Chemistry and Physics*, 19(6), 4025-4039, doi:10.5194/acp-19-4025-2019.

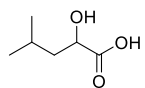
Table 1. Particle number concentration (N), mean diameter (D_p), total organic carbon (TOC) and total iodine (TI) of new particles with a residential time of 67 min in the bag reactor in the ozonolysis experiments and OH-enhanced experiment (dynamic mode). Those of 10-56 nm new particles collected by a nano Micro-Orifice Uniform Deposit Impactor (nano-MOUDI, MSP, Inc.) during an I-NPF event at a coastal site of Ningbo, China (Yu *et al.*, 2019) were also listed.

	TOC ($\mu\text{g m}^{-3}$)	TI ($\mu\text{g m}^{-3}$)	TOC/(TI+TOC)	N (cm^{-3})	D_p (nm)
ozonolysis experiments	45.6 \pm 9.7	0.88 \pm 0.34	96.1 \pm 2.9%	(5.58 \pm 2.04) $\times 10^4$	102 \pm 23
OH-enhanced experiment	125.3	9.5	92.9%	4.16 $\times 10^5$	73
I-NPF event at a coastal site of China	0.7	0.0135	98.2%	6.00 $\times 10^5$	16

Table 2. Major volatile organic compounds emitted by macroalgae as potential NPF precursors, sorted by TIC peak area measured by GC/MS or MS peak intensity measured by iodide-CIMS

	Formula	Structure	Peak area/MS peak intensity
1	C ₅ H ₁₂		1.90×10 ⁶
2	C ₅ H ₁₀		1.59×10 ⁶
3	CH ₃ I		1.37×10 ⁶
4	C ₃ H ₇ I		7.60×10 ⁵
5	CHBr ₃		4.71×10 ⁵
6	C ₅ H ₁₁ I		3.75×10 ⁵
7	CHBr ₂ Cl		2.71×10 ⁵
8	CH ₂ Cl ₂		2.55×10 ⁵
9	C ₁₀ H ₁₆		2.26×10 ⁵
1	C ₂ H ₆ O		1.70×10 ⁷
2	C ₃ H ₆ O		1.38×10 ⁷
3	C ₄ H ₆ O ₂		1.30×10 ⁷
4	C ₆ H ₁₂ O		1.03×10 ⁷
5	C ₅ H ₁₀ O		1.00×10 ⁷
6	C ₄ H ₁₀ O		5.16×10 ⁷
8	C ₂ H ₄ O		3.46×10 ⁷
9	C ₆ H ₁₀ O		2.88×10 ⁷
7	C ₅ H ₈ O		1.45×10 ⁷
10	C ₄ H ₈ O		1.37×10 ⁷
1	CH ₂ O ₂		1.58×10 ⁶
2	C ₂ H ₄ O ₂		9.52×10 ⁵
3	C ₃ H ₆ O ₃		9.21×10 ⁵
4	C ₆ H ₁₀ O ₃		4.44×10 ⁵
5	C ₂ H ₆ O ₂		2.88×10 ⁵
6	C ₄ H ₈ O ₂		1.17×10 ⁵

7

 $\text{C}_6\text{H}_{12}\text{O}_3$  1.12×10^5

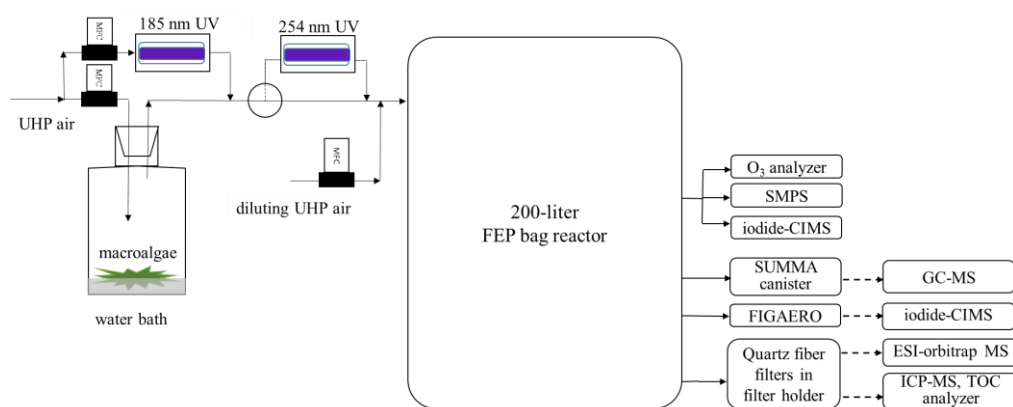


Figure 1. Schematic of experimental setup. Solid line: air flows. Dashed lines: sent for offline chemical analysis.

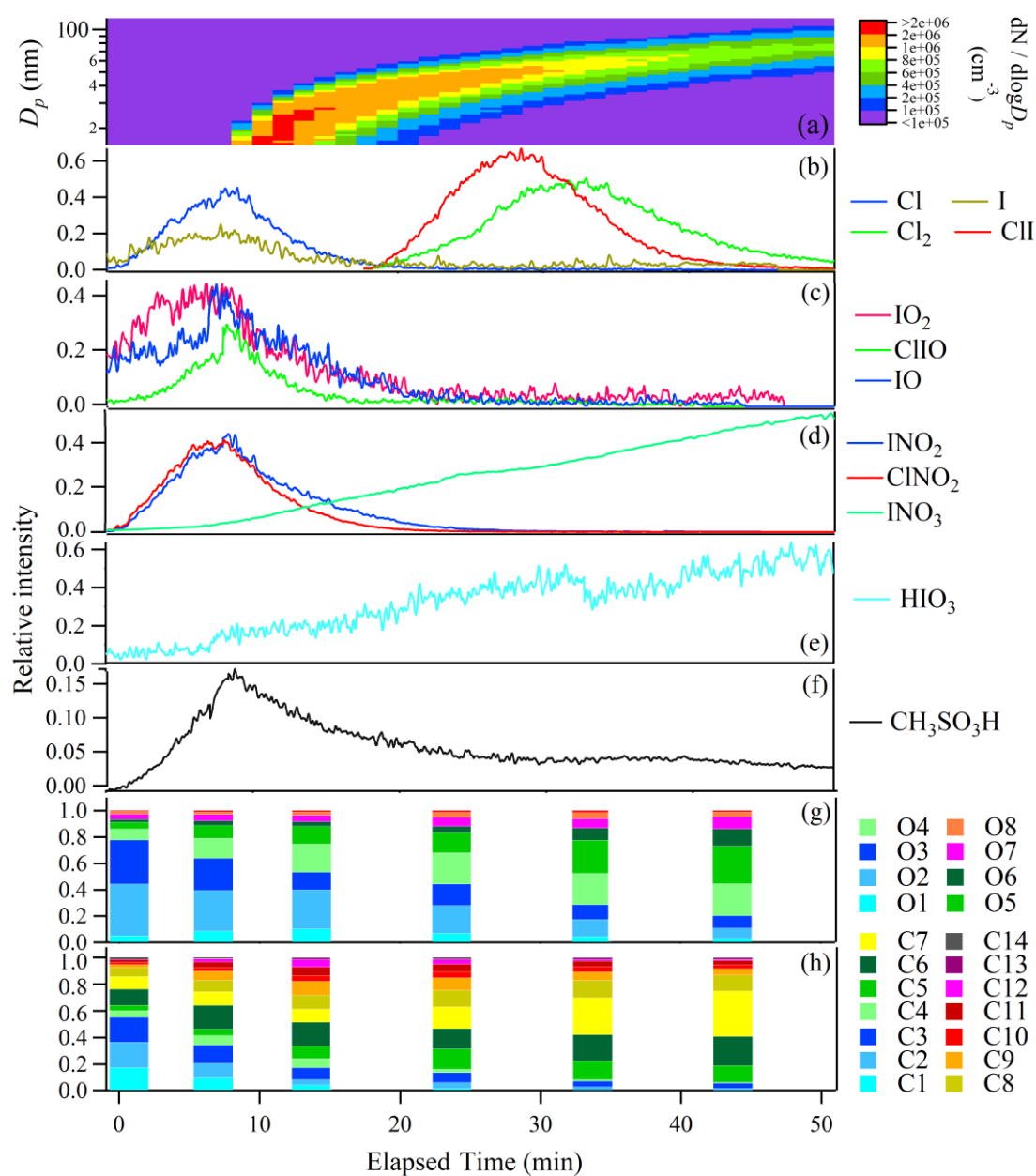


Figure 2. Time evolution of particle number size distribution (a) and relative intensities of gaseous molecules and radicals (b-f); the fractions of organic compounds grouped by O and C atom numbers in the selected time points (g-h) in a typical ozonolysis experiment (static mode). Time zero was chosen as the start time when HIO₃ was observed.

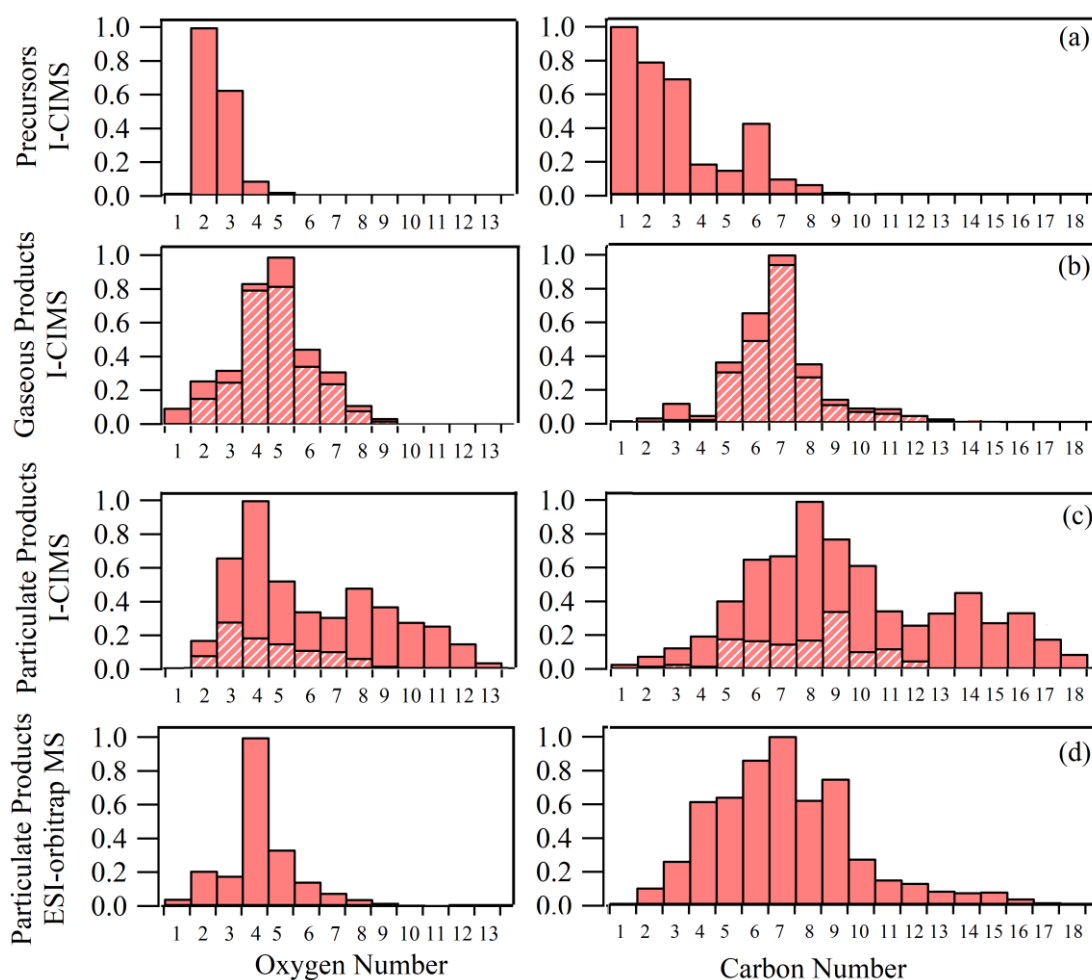


Figure 3. Oxygen and carbon atom number distributions of potential VOC precursors (a), gaseous products (b) and particulate products measured by iodide-CIMS (c), as well as the particulate products measured by ESI-orbitrap MS (d) in a typical ozonolysis experiment (dynamic mode). Hatched bars indicate the fractions of organic formulas observed in both gas and particle phases by iodide-CIMS.

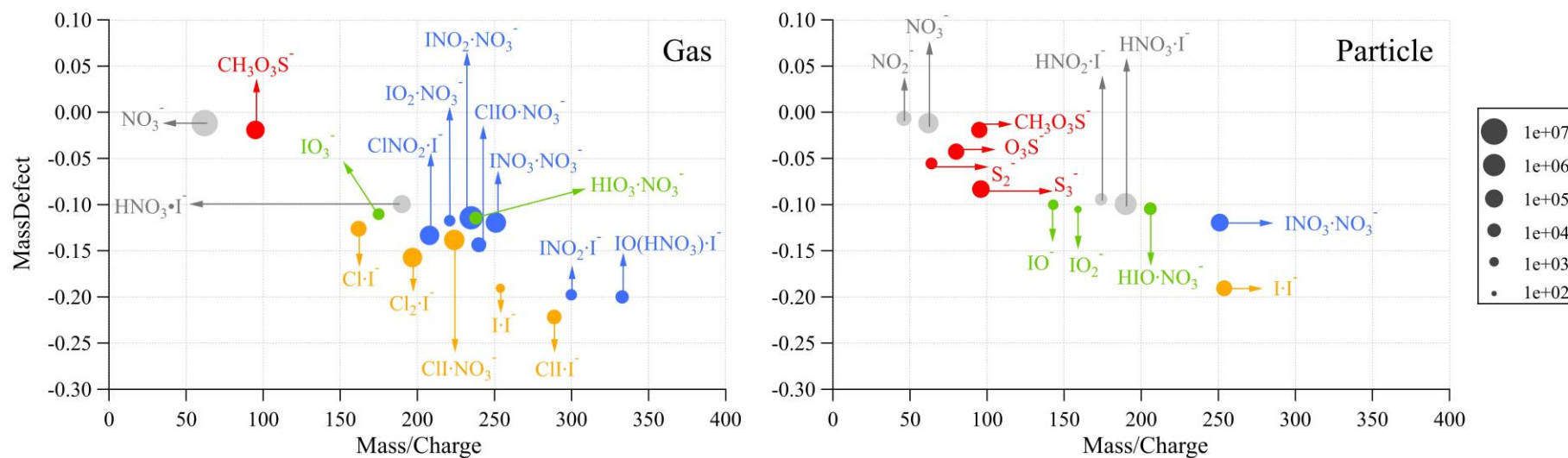


Figure 4. Integrated ion intensities of inorganic molecules and radicals in the gas phase (static mode) and particle phase (dynamic mode) measured by iodide-CIMS in a typical ozonolysis experiment. The ions were coded in color according to their elemental composition